

---

*Research Article: New Research | Sensory and Motor Systems*

## **Effect of circuit structure on odor representation in the insect olfactory system**

<https://doi.org/10.1523/ENEURO.0130-19.2020>

**Cite as:** eNeuro 2020; 10.1523/ENEURO.0130-19.2020

Received: 4 April 2019

Revised: 10 February 2020

Accepted: 23 February 2020

---

*This Early Release article has been peer-reviewed and accepted, but has not been through the composition and copyediting processes. The final version may differ slightly in style or formatting and will contain links to any extended data.*

**Alerts:** Sign up at [www.eneuro.org/alerts](http://www.eneuro.org/alerts) to receive customized email alerts when the fully formatted version of this article is published.

Copyright © 2020 Rajagopalan and Assisi

This is an open-access article distributed under the terms of the Creative Commons Attribution 4.0 International license, which permits unrestricted use, distribution and reproduction in any medium provided that the original work is properly attributed.

1 **Effect of circuit structure on odor representation in the insect**  
2 **olfactory system**

3  
4 Adithya Rajagopalan<sup>1</sup> and, Collins Assisi<sup>2</sup>

5 <sup>1</sup> *Janelia Research Campus, Howard Hughes Medical Institute, Ashburn, United States*

6 <sup>2</sup> *Division of Biology, Indian Institute of Science Education and Research, Pune, India*

7  
8 **Running title: Effect of circuit structure on odor representation.**

9  
10 **Corresponding Authors** Adithya Rajagopalan and Collins Assisi

11 **Email** [rajagopalana@janelia.hhmi.org](mailto:rajagopalana@janelia.hhmi.org), [collins@iiserpune.ac.in](mailto:collins@iiserpune.ac.in)

12 **Number of figures** 5

13 **Number of tables** 1

14 **Number of words in abstract** 247

15 **Number of words in introduction** 916

16 **Number of words in the discussion** 763

17  
18 **Conflict of Interest** The authors declare no competing financial interests.

19  
20 **Acknowledgements**

21 CA was funded by DBT–Wellcome Trust India Alliance through an Intermediate Fellowship IA/I/11/2500290  
22 and IISER Pune. AR was funded by an Inspire fellowship, Department of Science and Technology, India. We  
23 thank members of the Nadkarni and Assisi labs and Dr. Aurnab Ghose for useful discussions.

53 **Abstract**

54 In Neuroscience, the structure of a circuit has often been used to intuit function – an  
55 inversion of Louis Kahn's famous dictum, 'Form follows function' (Kristan and Katz 2006).  
56 However, different brain networks may utilize different network architectures to solve  
57 the same problem. The olfactory circuits of two insects, the Locust, *Schistocerca*  
58 *americana*, and the fruit fly, *Drosophila melanogaster*, serve the same function – to  
59 identify and discriminate odors. The neural circuitry that achieves this shows marked  
60 structural differences. Projection neurons (PN) in the antennal lobe (AL) innervate  
61 Kenyon cells (KC) of the mushroom body (MB). In locust, each KC receives inputs from ~  
62 50% PNs, a scheme that maximizes the difference between inputs to any two of ~50,000  
63 KCs. In contrast, in drosophila, this number is only 5% and appears sub-optimal. Using a  
64 computational model of the olfactory system, we show the activity of KCs is sufficiently  
65 high-dimensional that it can separate similar odors regardless of the divergence of PN-  
66 KC connections. However, when temporal patterning encodes odor attributes, dense  
67 connectivity outperforms sparse connections.

68 Increased separability comes at the cost of reliability. The disadvantage of sparse  
69 connectivity can be mitigated by incorporating other aspects of circuit architecture seen  
70 in drosophila. Our simulations predict that drosophila and locust circuits lie at different  
71 ends of a continuum where the drosophila gives up on the ability to resolve similar odors  
72 to generalize across varying environments, while the locust separates odor  
73 representations but risks misclassifying noisy variants of the same odor.

74 **Significance Statement**

75 How does the structure of a network affect its function? We address this question in the  
76 context of two olfactory systems that serve the same function, to distinguish the  
77 attributes of different odorants, but do so using markedly distinct architectures. In the  
78 locust, the probability of connections between projection neurons and Kenyon cells - a  
79 layer downstream - is nearly 50%. In contrast, this number is merely 5% in drosophila.  
80 We developed computational models of these networks to understand the relative  
81 advantages of each connectivity. Our analysis reveals that the two systems exist along a  
82 continuum of possibilities that balance two conflicting goals – separating the  
83 representations of similar odors while grouping together noisy variants of the same  
84 odor.

85 **Introduction**

87 Neural circuits encode a variety of stimuli and perform a wide range of computations.  
88 The structure of the neural circuit (i.e., the organization and statistics of the connectivity  
89 between neurons in the circuit) plays a key role in restricting the kinds of computations  
90 that the circuit can perform (Marr 1969, Albus 1971, Hopfield and Tank 1986).  
91 Understanding what different structural organizations imply for circuit function is an  
92 integral step towards generating a complete picture of brain function. These structure-  
93 function relationships are of particular interest in circuits that are trying to accomplish  
94 the same overarching goal while making use of different structural parameters. What  
95 advantages do the different parameter regimes provide in such situations? One such  
96 instance that has been explored recently, (Jortner, Farivar, and Laurent 2007, Jortner  
97 2013, Litwin-kumar et al. 2017) is the functional effect of different densities of

98 connections across species in the antennal lobe - mushroom body circuit of the insect  
99 olfactory system.

100

101 *Figure 1 caption: A schematic of the insect olfactory system*

102 *A schematic of the olfactory system contrasting the structural parameters of the*  
103 *circuit in a) *Drosophila melanogaster* and b) *Schistocerca americana*.*

104

105 The insect olfactory system is arguably one of the most well-characterized neural  
106 circuits.

107 Its compactness and simplicity, combined with the powerful genetic tools available, have

108 allowed a detailed understanding of its structure and function. The circuit begins at the

109 olfactory sensory neurons (OSNs) that convert odorant information from the

110 environment into electrical signals that are passed on to higher brain regions (Hallem

111 and Carlson 2004, 2006; Fisek 2014). The second level of the circuit is the Antennal Lobe

112 (AL), where the principal excitatory neurons - Projection Neurons (PNs) - represent odors

113 as dense spatiotemporal firing patterns (Laurent 1996b; Wehr and Laurent 1996; Wilson

114 and Laurent 2005). The AL then feeds information to the Mushroom Body (MB), where

115 Kenyon Cells (KCs) represent the odor as a spatially and temporally sparse pattern of

116 firing (Javier Perez-Orive et al. 2002; Turner, Bazhenov, and Laurent 2008). A high spiking

117 threshold and inhibitory inputs to KCs from a pair of large GABAergic neurons

118 (Papadopoulou et al. 2011; Masuda-Nakagawa et al. 2014, Lin et al. 2014) maintains the

119 sparseness of KC responses. The inhibitory GABAergic neurons are graded neurons

120 whose membrane voltage is mediated by the activity of the KCs, thus forming a feedback

121 inhibition loop [Figure 1]. Synapses immediately downstream of the KCs are plastic and

122 thought to be the primary locus of associative memory in the insect (Heisenberg 2003,  
123 Hige, Aso, Modi, et al. 2015). KCs converge on to the Mushroom Body Output Neurons  
124 (MBONs). From the MBONs onwards, neuronal activity is related more with behavioral  
125 output than with stimulus representation (Aso et al. 2014; Hige, Aso, Rubin, et al. 2015).  
126 While the overarching goal of the MB circuit - to distinctly represent odors so as to  
127 facilitate learning and appropriate behavioral responses - appears to be conserved  
128 across species, the number of connections received from the AL to a given KC varies  
129 significantly. In the fruit fly, a sparse ~5% of all PNs synapse onto each KC, whereas in  
130 the locust, this number is dense (~50%) [Figure 1] (Caron et al. 2013; Jortner, Farivar and  
131 Laurent 2007). 50% connectivity seen in the locust olfactory system is thought to  
132 maximize the differences between the inputs received by individual KCs (Jortner, Farivar,  
133 and Laurent 2007; Jortner 2013). 5% connectivity observed in drosophila, must then  
134 make it a sub-optimal classifier. The combinatorial arguments that have been posited  
135 thus far do not consider the full spatiotemporal extent of an odor-evoked pattern of  
136 activity in the antennal lobe. To understand the implications of these contrasting  
137 connectivities, we tested the response of the fly and the locust olfactory networks to  
138 two different kinds of inputs – one, where odors were represented as spatiotemporal  
139 patterns of activity by AL neurons and another, where odors were represented only by  
140 the identity of active PNs. We show that an identity code allows a broad range of  
141 connection densities, including those seen in both the fly and locust, to distinguish  
142 different odors. However, with temporal variations, denser connectivities between PNs  
143 and KCs maximize the distance between odor representations. The sensitivity of the  
144 locust olfactory system, due to its dense connectivity, comes at a cost. Under changing  
145 environmental conditions, the same odor may generate different representations in PN

146 space that the locust could potentially misclassify as distinct odors. Such  
147 misclassifications are less likely in the drosophila circuit where PN-KC connections are  
148 sparse. To elucidate the logic behind these connectivities, we simulated the distinct  
149 architectures of each insect. In drosophila, all the sensory neurons expressing a  
150 particular receptor type synapse onto PNs in a spatially circumscribed structure called a  
151 glomerulus. Sister PNs, that receive inputs from ORNs at a particular glomerulus, tend to  
152 fire in a highly correlated manner (Kazama and Wilson 2009) (though this is not the case  
153 in related mammalian cells –(Dhawale et al. 2010) where the activity, though correlated  
154 is different). In contrast, locust glomeruli receive input from multiple ORN types. We  
155 show that the glomerular architecture of the fruit fly improves the ability of the network  
156 to distinguish odors despite a low probability of PN-KC connections. Our simulations  
157 predict that the fruit fly and locust circuits lie at different ends of a continuum where the  
158 fruit fly gives up on resolution in odor space so that it can generalize across varying  
159 environments. This implies that very similar odors may be misclassified as the same odor  
160 as they are too similar to be resolved. The locust, on the other hand, maximally  
161 separates odor representations but runs the risk of misclassifying the same odor under  
162 different conditions.

163

## 164 **Methods**

### 165 **Temporally patterned odor representations in AL circuits**

166 We modeled the odor representation in the AL in two ways. First, as a static  
167 representation consisting of a binary vector of length 900 (number of model PNs). Each  
168 element of the vector indicated only whether a particular PN was active (if the value at

169 that position was 1) or not (0) [Figure 2a]. The second representation incorporated the  
170 temporal evolution of the odor. In the locust AL, odors elicit a temporal pattern of  
171 activity in PNs that begins with the onset of the odor. In experimental recordings, not all  
172 PNs show an odor specific response that begins immediately upon odor onset. Several  
173 neurons show increased activity many milliseconds after odor onset. Some PNs can  
174 show complex responses such as an increased level of activity to both odor onset and  
175 offset. However, it is likely that the onset and offset responses are largely seen in  
176 nonoverlapping groups of PNs (Saha et al. 2017). Here, we simulated PN spiking activity  
177 as continuous bursts. The spatiotemporal pattern generated by the PN population was  
178 defined by the onset, offset, and duration of PN bursts. Another important aspect to  
179 consider was the presence of oscillations in the Local Field Potential (LFP) in the 20-  
180 30Hz frequency range (Laurent 1996a) in the AL of locusts. Similar oscillations have also  
181 been observed in intracellular recordings from drosophila AL (Tanaka, Ito, and Stopfer  
182 2009). The presence of such oscillations suggests that odor induced PN responses are  
183 correlated with more PNs spiking at the peak of the LFP than at other phases. The  
184 oscillations also provide a natural time scale to partition the PN response into smaller 50  
185 ms epochs (the duration of one cycle at 20Hz). We measured the time to odor initiation  
186 and the duration of a continuous PN response in units of epochs. The statistics of the  
187 number and timing of PN spikes were extracted from a survey of the literature (see table  
188 1 - Laurent 1996b; Wehr and Laurent 1996; Stopfer, Jayaraman and Laurent, 2003;  
189 Wilson and Laurent 2005). We adapted these results to design a matrix representation  
190 of PN activity. This consisted of a 900x3000 matrix of 1s and 0s [Figure 3]. Each row  
191 represented one out of 900 PNs, and each column of the matrix represented the activity  
192 of all PNs over a 1ms time interval. The parameters (and their values) used in this



193 process (to simulate 1 second of odor delivery and a 3-second response) are listed below  
 194 (note all variables are normally distributed, and values represent mean  $\pm$  standard  
 195 deviation unless mentioned otherwise):

196 Table 1: Statistics of PN spikes

Percentage of active neurons	$(0.2 \pm 0.05) \times$ number of PNs
Basal firing rate	$3.87 \pm 2.23$ spikes/second.
Odor induced firing rate	$19.53 \pm 10.67$ spikes/second
Number of active epochs	$8 \pm 4$ cycles of <u>LFP</u>
Number of epochs before activity	Number of LFP cycles drawn from a uniform integer distribution ranging from 1 to 20

197  
 198 To generate a population PN response, a value used to specify the percentage of active  
 199 neurons was drawn from a normal distribution with mean and variance given in Table 1.  
 200 This value was used as a probability threshold to decide if a given PN fires or not. For  
 201 each of the 900 PNs, a uniform random number was drawn to decide whether that PN  
 202 was activated by the odor. If the random value was less than the probability threshold  
 203 chosen, then the neuron was activated by the odor. A value of the basal firing rate (per  
 204 second) was drawn from a normal distribution with the appropriate mean and standard  
 205 deviation (Table 1) and spikes equaling three times the value drawn were uniformly and  
 206 randomly distributed over the 3000 time points. A value for odor induced firing rate was  
 207 drawn from a normal distribution, as were the number of active epochs and the number

208 of epochs before odor-induced activity. These three values provide information about  
209 which of the LFP oscillation cycles additional spikes needed to be added to the particular  
210 neuron's activity, as well as how many spikes were to be added in a single epoch. These  
211 spikes were then distributed in each of the "active" epochs in such a way that the spike  
212 was more likely to occur at the center of the epoch (corresponding to the peak of the  
213 LFP) than at the ends. If the neuron was not odor-activated, then it fired at its basal  
214 firing rate as described earlier.

215 These attributes were calculated for each of the 900 PNs to generate a complete  
216 spatiotemporal pattern describing an odor. An odor was defined by the specific PNs that  
217 were activated and the parameters drawn from the distributions quantified in Table 1. In  
218 different trials of the same odor, the PNs that were activated, as well as their  
219 parameters, remained the same. However, the exact timing of the spikes in the active  
220 epochs changed.

221 The timing of spikes was drawn randomly (within specified "active" epochs) for each  
222 trial. In contrast, two odors differ not only in the timing of spikes of active PNs but also  
223 in the identity of the active PNs.

224 Whether a PN was active or not was independent of whether other PNs were active. This  
225 reflected the multi-glomerular organization seen in locust. To mimic a fly-like glomerular  
226 organization where sister PNs fire in a correlated manner, PNs were divided in 50 groups  
227 of 6 (Note that here we simulated 300 PNs and not 900 in agreement with the number  
228 seen in the fly). The grouping reflected the glomerular architecture in *Drosophila*. 5 out  
229 of these 50 groups were chosen to contain active neurons. The other 4 parameters  
230 mentioned in Table 1 were then chosen for these active neurons. To simulate a new

231 odor that was distinct from a previously described one, 1-5 of the active glomeruli in the  
 232 first odor were changed randomly (See Figure 3 for an instance of a simulated odor).

### 233 **Neuron and synapse implementation**

234 The spatiotemporal pattern that was generated using specific attributes for PN spike  
 235 statistics described above was used to stimulate a layer of 50,000 KCs. We systematically  
 236 varied PN-KC connections and computed the corresponding KC responses to several  
 237 odors. PN-KC synapses are cholinergic (Yasuyama 1999) and were modeled as such  
 238 [equations 1, 2, 3] (Destexhe, Mainen, and Sejnowski 1994; Bazhenov et al. 2001; Javier  
 239 Perez-Orive et al. 2002; Turner, Bazhenov, and Laurent 2008). Each PN spike released a  
 240 fixed amount of neurotransmitter T. This was used to drive post-synaptic KCs. The  
 241 synaptic currents were given by:

$$242 \quad I_{syn} = g_{syn} \times [O] \times (V - E_{syn}) \quad (1)$$

243

244 Where,

$$245 \quad \frac{d[O]}{dt} = \alpha \times (1 - [O]) \times T - \beta \times [O] \quad (2)$$

$$246 \quad T = A \times \Theta \times (t_0 + t_{max} - t) \times (t - t_0) \quad (3)$$

247

248 In these equations the constants were:

$$249 \quad \alpha = 0.94 \text{ ms}^{-1}, \beta = 0.18 \text{ ms}^{-1}, g_{syn} = 0.05 \frac{mS}{cm^2}, E_{syn} = 0 \text{ mV and } t_{max} = 0.3 \text{ ms} . \quad \Theta \text{ is the}$$

250 Heaviside function.  $[O]$  is the open probability of the ion channels on the KC membrane  
 251 and  $T$  represents the amount of neurotransmitter released by a given PN.  $t_0$  is the time  
 252 of the last spike and  $t_{\max}$  is the duration for which the neurotransmitter was released.  
 253 KCs were modeled as leaky integrate and fire neurons (Turner, Bazhenov, and Laurent  
 254 2008; Papadopoulou et al. 2011).

$$255 \quad C_m \frac{dV}{dt} = -g_L(V - E_L) - I_{syn} \quad (4)$$

256 Here  $g_L = 0.089 \frac{\text{mS}}{\text{cm}^2}$ ,  $C_m = 1 \frac{\mu\text{F}}{\text{cm}^2}$  and  $E_L = -65 \text{ mV}$ . The KC generated a spike when  
 257  $V > V_{\text{thresh}}$ . The membrane potential was reset to  $-65$  mV at the time point immediately  
 258 after the spike. We simulated an array of 50,000 such KCs that responded to a 3000ms  
 259 long input from PNs.

## 260 **Classification and distance metrics**

262 To quantify the difference between the representations of two odors by the same  
 263 neuronal population we used the Hamming distance. Elements of the KC activity vector  
 264 were set to 1 if that KC fired a spike during the odor presentation and zero otherwise.  
 265 The Hamming distance calculates the number of bits that differ between the two vectors  
 266 (For example see Figure 2). In some figures, we used a normalized version of this metric  
 267 that divides twice the Hamming distance by the total number of active neurons in both  
 268 vectors being compared. To illustrate this metric, consider a vector representing the  
 269 activity of 100 neurons. Consider, in one scenario 10 of these neurons were active for  
 270 odor A and a different set of 10 non-overlapping neurons for odor B. The Hamming  
 271 distance between these odor representations would be 20. In another scenario, 20

272 neurons were activated for odor A and 20 non-overlapping neurons for odor B, the  
273 Hamming distance would be 40. However, in both cases the two odors were maximally  
274 different from one another, that is, they did not overlap. In contrast, the normalized  
275 Hamming distance for both cases described above would take a maximum value of 1.  
276 The normalized Hamming distance may be thought of as a measure of the degree of  
277 overlap between odor representations. If two odors stimulate strictly non-overlapping  
278 KCs the distance between the representations would be 1 regardless of the number of  
279 active KCs. This normalization was also necessary to visualize the distance between odor  
280 representations particularly when the PN-KC connections were dense (>50%). Dense  
281 connectivity regimes showed a large trial-trial variation in the number of active KCs.

282 In addition to using the normalized Hamming distance to visualize the distance between  
283 odor representations, we used two classification algorithms (k-medoids clustering and  
284 non-classical multidimensional scaling) to visualize and classify high dimensional KC  
285 representations of odors. In both these classification algorithms we first defined the  
286 pairwise Hamming distance between the KC vectors of all simulated odor  
287 representations. The algorithm (k-medoids clustering using MATLAB) iteratively  
288 minimizes the within cluster distance while maximizing the distance across clusters.

289 Unlike the k-means clustering algorithm that calculates a center for each cluster as the  
290 mean of the cluster, the k-medoids algorithm treats an existing data point as the center  
291 of the cluster and measures all within-cluster distances from that point. We also  
292 performed a multidimensional scaling analysis using the mdscale function in MATLAB.  
293 The algorithm maps points from the high-dimensional KC space to a plane while  
294 preserving the pairwise distance relationship between all the data points.

295 **Code Accessibility**

296 The code/software described in the paper is freely available online at  
297 <http://modeldb.yale.edu/261877> . The access code for the online repository is 0000. The  
298 code is also available as Extended Data.

299 **Results**

300 In the locust, each KC receives input from nearly half of the antennal lobe PNs. This  
301 pattern of connectivity maximizes the difference between inputs to any two of the  
302 ~50,000 Kenyon cells in the mushroom body [Figure 2b] (Jortner, Farivar, and Laurent  
303 2007). Given the large number of possible combinations of inputs to KCs, it is highly  
304 unlikely that the combination of PNs that synapse onto a given KC will be exactly the  
305 same as that which synapse onto any other KC. In contrast, if the PN-KC connection  
306 probability were 5% (seen, for example, in drosophila), the number of total possible PN  
307 combinations would be nearly 99% lower than if the PN-KC connection probability were  
308 50%, making it more likely for two KCs to share the same inputs [Figure 2b], (Jortner,  
309 Farivar, and Laurent 2007, Jortner 2013). What advantages does this seemingly sub-  
310 optimal scheme offer? We addressed this conundrum by simulating a model KC network  
311 that received realistic PN input. Using the distance between KC odor representations,  
312 and the classification accuracy of the network, as a proxy for the ability of the animal to  
313 distinguish odors, we determined the circumstances under which different circuit  
314 connectivities confer specific advantages in odor discrimination.

315  
316 **A PN identity code allows a wide range of connectivities to distinctly represent odors**

317 If each KC sees  $m$  out of  $n$  PNs, then the maximum number of combinations would be

318 obtained for  $m = \frac{n}{2}$  [Figure 2b]. However, it is the response of KCs that is read by  
319 subsequent layers, not PN input. The KC response may be thought of as a nonlinear  
320 transformation of the summed input from the PNs. KCs act as coincidence detectors that  
321 integrate pre-synaptic input that arrives within short temporal windows of the order of  
322  $\sim 50$ ms (Perez-Orive J. et al. 2004, Perez-Orive J. et al. 2002, Gruntman & Turner 2013).  
323 KCs fire only if a sufficient number of spikes fall within the integration window.  
324 Therefore, we first investigated whether the previously hypothesized (Jortner, Farivar,  
325 and Laurent 2007) optimal connection probability from PNs to KCs remains optimal in  
326 spite of the threshold imposed by the KC response and whether a lower connection  
327 probability is indeed sub-optimal. <sup>SM</sup>

328 Figure 2 caption: *50% connectivity does not maximally separate KC representations when*  
329 *PN inputs are static*  
330 *a) The threshold model of KCs. The left-most vector represents the PN activity. This is*  
331 *combined through a connectivity matrix to give the input seen by each KC (a 50000-*  
332 *element long vector). Thresholding is then applied to define spiking KCs. b) The Hamming*  
333 *distance between inputs seen by two KCs is calculated for all possible pairs and averaged*  
334 *and plotted as a function of the PN-KC connectivity. c) The mean ( $\pm$  standard deviation)*  
335 *normalized Hamming distance between the activity of KC networks driven by two*  
336 *different inputs is plotted on the y-axis as a function of the PN-KC connectivity. Different*  
337 *shades plot the distance between odor representations that differed in 5-80% of the*  
338 *active PNs.*  
339

340 We tested this hypothesis using a simple threshold model of KCs and determined how  
341 distinctly the KC population output represented different odors. We modeled the input  
342 to KCs as a binary vector of length 900. This captured a single snapshot of the activity of  
343 the AL circuit (Jortner 2013; Litwin-kumar et al. 2016) [Figure 2a]. In the locust AL, the  
344 duration of each cycle of the 20 Hz oscillatory local field potential provides a natural  
345 time-scale to define the duration of a snapshot. We then calculated the response of KCs

346 to this input for different values of PN-KC connectivity. We varied the number of  
347 projections from PNs to KCs such that each KC received inputs from 5 to 95 percent of all  
348 PNs (in steps of 5 percent). We simulated different odors by randomly shuffling the PN  
349 activity vector. If the summed activity of all the PNs that were connected to the same KC  
350 exceeded a threshold, we labeled the KC as active and set its response to 1. Increasing  
351 the density of connections from PNs to KCs increased the number of active KCs for the  
352 same input vector. Changes in the sparseness of the KC output vector can lead to a  
353 change in the distance between odor representations. Our goal was to calculate the  
354 overlap between output vectors, independent of the sparseness of the representation.  
355 Therefore, for each connection probability we adjusted the response threshold of KCs  
356 such that only 10% of the 50,000 KCs simulated crossed the threshold. (Javier Perez-  
357 Orive et al. 2002; Turner, Bazhenov, and Laurent 2008). This ensured that changes in the  
358 distance between odor representations were solely due to changes in the PN-KC  
359 connectivity and not confounded by connectivity dependent changes in the sparseness  
360 of the KC response. We simulated four sets of inputs consisting of 101 PN odor  
361 representations. Within each of the four sets of simulated odors, the input vectors  
362 differed from each other by varying amounts - 5, 10, 20, 40 or 80% respectively. For  
363 example, consider the 900 PNs whose activity represented a given odor 'A'. About 20%  
364 of these PNs would be active. Another odor 'B' in the input set would differ from 'A' by  
365 10% if 90 of the 900 PNs changed their activity state from active to inactive or vice versa  
366 when compared with 'A'. We then calculated the normalized Hamming distances  
367 between odor pairs belonging to each group and compared the distances obtained for  
368 different PN-KC connection probabilities. The KC population's ability to distinctly  
369 represent odors showed no dependence on the connectivity between the two regions



370 [Figure 2c] regardless of the degree of similarity between the PN representations of  
371 odors. This counterintuitive result arises from the fact that even at low connectivity  
372 values the number of ways to choose inputs to KCs is more than a hundred orders of  
373 magnitude greater than the number of KCs in the network (Litwin-kumar et al. 2016)(see  
374 the Discussions section). Therefore, when odor distances were measured in terms of the  
375 output of KCs, both the drosophila (5% PN-KC connectivity) and the locust olfactory  
376 network (50% connectivity) were equally capable of distinguishing between similar  
377 odors.

378 **Inclusion of PN temporal patterning reveals the functional differences between**  
379 **connectivities**

380 In response to an odor presentation, AL neurons generate a dynamic pattern that  
381 evolves reliably and over multiple time scales. This spatiotemporal patterning is thought  
382 to progressively decorrelate the representations of similar odorants (Wiechert et al.  
383 2010) and make them more easily discriminable by follower neurons in the mushroom  
384 body. Earlier, we used a single snapshot in time to represent an odor and found that the  
385 PN-KC connectivity had little effect on the Hamming distance between KC  
386 representations of the odor. Next, we sought to determine the role of the temporal  
387 structure of odor representations in discrimination.

388 *Figure 3: Simulation of temporally patterned PN inputs to a KC network.*  
389 *a) The matrix on the left represents the activity of a set of 900 PNs. Each row shows*  
390 *the activity of a single PN during a 3000ms time period. Blue dots show the time of a*  
391 *spike. The red region represents the time during which the odor was presented. On*  
392 *top, a summation of the activity of the entire PN network is shown clearly indicating*  
393 *the oscillations in the net PN activity. This input was used to calculate  $T$  and  $I_{syn}$  (the*  
394 *synaptic input to KCs). The differences between the population representation of two*  
395 *inputs were calculated using the Hamming distance. b) Mean population response of*  
396 *900 PNs projected onto the first three principal components for three odors is shown*  
397 *by the black traces. Individual trials are shown by the colored traces c) The mean*

398 *membrane potential of all KCs shows a 20Hz oscillation. Bottom panels show the*  
399 *response of two KCs (in red and black traces) to two different odors. Only the first*  
400 *odor evokes a consistent response from this particular KC across 5 odor trials (middle*  
401 *panel). The second odor does not lead to reliable spiking in this example KC.*  
402

403 Odor inputs to KCs were modeled as a pattern of spikes from PNs. The statistics of spikes  
404 emulated that seen in the extant literature (see methods). We simulated trial-trial  
405 variability by jittering the spike timing within 50 ms windows. Note that in addition to  
406 this jitter, random spikes were inserted such that the mean baseline firing rate in the  
407 absence of an odor stimulus was 4 Hz. We simulated different odors by activating  
408 different groups of PNs. To visualize the dynamics of the population of PNs, we first  
409 calculated the number of spikes generated by each PN in overlapping 50 ms windows.  
410 We then projected the PN activity vector during each 50ms window onto the first three  
411 principal components. Odor representations of the PN population may be visualized as  
412 continuous trajectories in this reduced-dimensional space. When the odor stimulus was  
413 turned on, the AL response followed a trajectory from baseline (defined by low firing  
414 rates) to a 'fixed point' (Mazor & Laurent 2005). Once the odor stimulus was turned off,  
415 the trajectory returned to baseline, but along a different path from the one it had taken  
416 to reach the fixed-point post-odor-onset (Mazor & Laurent 2005, Stopfer et al. 2003).  
417 Multiple trials of the same odor generated trajectories that remained close to each  
418 other, while dissimilar odors were well separated in the space defined by the principal  
419 components. [Figure 3]. The input from PNs was used to drive a population of KCs. In  
420 contrast to the threshold model of KCs used in the previous section, here we modeled  
421 KCs as leaky integrate and fire neurons with integration properties that matched the  
422 responses seen in earlier studies (Javier Perez-Orive et al. 2002; J. Perez-Orive,  
423 Bazhenov, and Laurent 2004). Here too, we maintained the sparseness of KC responses

424 across different PN-KC connection regimes by choosing progressively higher spike  
425 thresholds as the probability of connections increased. The threshold chosen ensured  
426 that only 10% of the KCs spiked in each epoch (50ms window) when the odor was  
427 present regardless of the connectivity. We chose such a threshold-based sparseness to  
428 mimic the ultimate effect of the GGN that dynamically adjusts feedback inhibition in  
429 response to the intensity of the KC response. However, for high PN-KC connectivity,  
430 (>50%), we found that the difference between inputs to different KCs was very small.  
431 Therefore, small changes in the KC threshold led to an all-or-none response and  
432 consequently a high variability across trials and a reduced ability to discriminate  
433 between odorants. Intrinsic variability in KC thresholds and differences in the strengths  
434 of PN-KC synapses can potentially reduce this variability for connectivities beyond 50%.  
435 We used a normalized Hamming distance to visualize differences across all connectivity  
436 values. In the 0-50% connectivity regime, where the number of activated KCs remained  
437 nearly the same and well-controlled by KC threshold modification, the Hamming  
438 distance matched the normalized Hamming distance except for a constant scaling factor.  
439 Including PN temporal patterning revealed some functional differences between  
440 different PN-KC connectivity regimes.  
441 KCs received inputs that represented odors with different degrees of similarity between  
442 them. We calculated the mean normalized Hamming distance between all pairs of KC  
443 activity vectors for different odors and connectivities [Figure 4a]. Our analysis began to  
444 pick out differences in the ability of the KC population with different connectivities to  
445 represent odors distinctly. The normalized Hamming distance between KC odor  
446 representations increased with increasing PN-KC connectivity for all odor distances

447 [Figure 4a]. This implied that the representations of two different odors are more  
448 distinct in higher connectivity regimes. This could potentially allow the network to  
449 accurately associate specific odors with reward signals in downstream layers of the  
450 olfactory circuit  
451 (Cassenaer & Laurent 2012, Oswald et al. 2015, Hige et al. 2015). However, an increase in  
452 Hamming distance was accompanied by a concomitant increase in the variability of the  
453 distance across odor pairs. We found a similar trend in the distance between the trials  
454 that represented the same odor (trace marked 0% difference in Figure 4a). Therefore,  
455 for high PN-KC connection densities, it seemed likely that different trials of the same  
456 odor could be incorrectly classified as distinct odors. Ideally, the network must maximize  
457 the distance between odor representations while also keeping the trial-trial variability  
458 within a range that prevents misclassification of odors. The Hamming distance metric  
459 does not take into account the variability of KC odor representation. Therefore, we used  
460 k-medoids clustering to separate the odor representations into non-overlapping groups.  
461 Our data consisted of 25 KC response vectors (5 odors x 5 trials). Each was a 50000-  
462 element long vector, where each element represented a single KC and contained either  
463 a 1 if that KC was active or 0 if it was inactive. We determined whether the trials had  
464 been grouped correctly based on their odor identity. For each set we used the  
465 percentage of correct classifications as a measure of the ability of the network to  
466 distinguish between odorants. As the PN-KC connectivity increased to nearly 45%, the  
467 number of correct classifications dropped abruptly, indicating that the distance across  
468 trials of the same odor matched or exceeded the distance between representations of  
469 different odors [Figure 4b]. Therefore, 45% PN-KC connectivity increased the distance  
470 between representations while keeping trial-trial variability within a reasonable range.

471 This result is similar to that of (Jortner 2013) though it is based on the output of KCs over  
472 a few seconds of odor stimulation, while (Jortner 2013) based their conclusion on a  
473 single snapshot of odor input. Next we used multidimensional scaling to visualize the  
474 distribution of different odors on a plane. The algorithm mapped each 50000-  
475 dimensional KC representations of an odor trial on to a single point on this plane. For  
476 low values of PN-KC connectivity, multiple trials of the same odor preferentially  
477 remained close together. As the divergence of connections increased, the separation  
478 between the representations of different trials of a particular odor and different odors  
479 began to merge, making it difficult to correctly segregate the odors [Figure 4c, different  
480 odors are marked in different colors]. The odors plotted here differed from each other in  
481 5% of the PNs that were stimulated.

482 It is possible that the differences in Hamming distance could be merely a consequence of  
483 using a specific KC model (an integrate-and-fire neuron here) compared to a nonlinear  
484 threshold neuron in earlier sections. To show that this is not the case we created odor  
485 representations in which odors differed only in the identity of PNs that they activated.  
486 All active PNs produced the same number of spikes at exactly the same points in time. In  
487 this way we continued to include all aspects of our expanded model but removed any  
488 differences in temporal structure that could be utilized differently by the different  
489 connectivity regimes. Therefore, if the usage of our new KC model that evolved in time  
490 was the cause for the functional differences that we saw, then the results of this  
491 simulation would differ from that of the previous simulations [Figure 2c] that used a  
492 threshold model. We found that the distance between odor representations in both  
493 models, the integrate and fire model and the threshold model, were independent of the

494 degree of PN-KC connectivity when temporal features of the odor representation were  
495 eliminated (compare Figure 4d with Figure 2c).

496 Taken together, these results suggest that the inclusion of temporal structure in AL  
497 activity causes post-synaptic KC populations that receive a large number of inputs to  
498 respond differently from those that receive few inputs. However, there appears to be a  
499 trade-off here. Dense connectivity regimes are highly sensitive to small changes in  
500 incoming input and can incorrectly categorize noisy trials of the same odor as different  
501 odors. On the other hand, sparse connectivity regimes produce reliable representations  
502 that can be clustered correctly into different groups. However, these are likely to fail if  
503 very similar odors are introduced because the representations may not be well  
504 separated as seen from the low Hamming distance between the odor representations  
505 [Figure 4].

506 Figure 4 caption: *PN temporal patterning reveals the functional differences between*  
507 *connectivities*

508 a) *Distance between odor representations. The mean ( $\pm$  standard deviation)*  
509 *normalized Hamming distance between the KC representations of odor pairs is shown as*  
510 *a function of the PN-KC connectivity value. Here KCs are modeled as described in*  
511 *Figure 3. b) Classification accuracy decreases with increasing PN-KC connectivity. A k-*  
512 *medoids clustering algorithm that used the distance between 25 KC activity vectors (5*  
513 *trials x 5 odors) was used to categorize each vector as one of 5 odors. The percentage of*  
514 *correctly classified odor representations is plotted on the y-axis as a function of the*  
515 *connectivity of the PN-KC network. c) Odor representations become indistinguishable*  
516 *with increasing PN-KC connectivity. Five odors that differed from each other by 5% PN*  
517 *input, mapped to a plane using multidimensional scaling. Different trials of a given odor*  
518 *are plotted using a single color. Different odors are plotted using different colors. The*  
519 *PN-KC connectivity is shown in the title of each sub-plot d) Hamming distance between*  
520 *static odor representations. The mean ( $\pm$  standard deviation) normalized Hamming*  
521 *distance between the KC representations of odor pairs is plotted as a function of PN-KC*  
522 *connectivity. Here, the PN odor representation did not change in time.*

### 523 **Glomerular organization of the fly aids odor discrimination**

524 Olfactory receptor neurons in insects are distributed randomly across the antennae  
525 within tiny hair like structures called sensilla. Each receptor neuron expresses a single

526 olfactory receptor protein and possesses a receptive field tuned to a variety of odorants  
527 (Hallem and Carlson 2004, 2006). In drosophila, all the sensory neurons expressing a  
528 particular receptor type synapse onto a single glomerulus giving nearly identical input to  
529 sister PNs that receive input from that glomerulus (Kazama and Wilson 2009). While  
530 correlated PN responses can potentially improve the signal to noise ratio, this comes at a  
531 cost, namely, the dimensionality of the olfactory representation is vastly reduced. The  
532 size of the representation may be thought of as the number of independent dimensions,  
533 that is, the number of neurons that can generate uncorrelated patterns of activity. In  
534 locusts that lack this glomerular organization, the maximum number of independent  
535 dimensions is 900 (number of PNs that could potentially receive unique odor input). In  
536 drosophila this reduces dramatically since multiple neurons receive identical input from  
537 ORNs and generate a highly correlated output. The number in drosophila may be much  
538 smaller (~50, the number of glomeruli) since the output of sister PNs is nearly the same.  
539 Does the glomerular organization of the drosophila olfactory system mitigate some of  
540 the disadvantages in odor discrimination imposed by sparse PN-KC connections?

541 *Figure 5: Glomerular organization of the fly aids odor discrimination*

542 *(a) The mean ( $\pm$  standard deviation) normalized Hamming distance as a function of PN-*  
543 *KC connectivity in a network with glomerular structure. (b) The normalized HD of odors*  
544 *with a 1-glomerulus difference in a fly-like glomerular system is compared to the HD*  
545 *between odor representations of a system with locust-like glomerular structure. (c)*  
546 *Classification accuracy of odors that are different by 2 glomeruli (2% or 12 neurons in the*  
547 *fly-architecture) (blue trace) compared to the classification accuracy of odors that*  
548 *differed by 5% (45 neurons) of stimulated odors in locust. Classification accuracy is higher*  
549 *for the fly-like organization for low PN-KC connectivities.*

550  
551 To test if the inclusion of the uni-glomerular architecture seen in the fly produces any  
552 improvement in the ability of sparsely connected networks we performed simulations in  
553 which odors were defined by the glomeruli they activated. These odors differed in the  
554 number of unique glomeruli they activated rather than the number of unique PNs



555 [Figure 5a]. These inputs were then fed to the same KC network simulated earlier. We  
556 saw that for sparse connectivity regimes the uni-glomerular organization magnified the  
557 differences in PN activity and increased the Hamming distance between KC  
558 representations of odors compared to the non-glomerular case [Figure 5b]. We then  
559 used k-medoid based clustering and classification to determine whether the fly-like  
560 architecture provided any benefits in odor classification. We compared the classification  
561 accuracy as a function of PN-KC connectivity for two cases – a system with a multi-  
562 glomerular (locust-like architecture) and one with a uni-glomerular (fly-like  
563 architecture). We found that the uni-glomerular architecture improved the classification  
564 accuracy of the network for low PN-KC connectivities compared to the multi-glomerular  
565 architecture [Figure 5c]. However, this kind of glomerularization appears to cause no  
566 change or even slightly reduce the ability of dense connectivity schemes to separate  
567 odor representations. This suggests that the glomerular organization seen in the fly does  
568 in fact improve the animal's ability to distinguish between odors.

569

## 570 **Discussion**

571 ***Discrimination of purely spatial odor representations is independent of PN-KC***

572 ***connection density***

573 In the locust AL, PNs generate elaborate spatiotemporal patterns in response to an odor.  
574 These patterns are read by KCs in the MB. The density of connections between PNs and  
575 KCs is such that each KC receives input from nearly one half of the PNs. A 50%



576 probability of connections from PNs to KCs ensures that the PN inputs to KCs are  
577 maximally separated. The number of ways to pick  $m$  out of  $n$  elements is maximized  
578 when  $m \approx \frac{n}{2}$ , thus maximizing the distance between inputs to KCs (see Figure 2b and  
579 Jortner 2013). This argument assumed that this distance between inputs dropped off  
580 quickly as  $m$  changed from  $m \approx \frac{n}{2}$ . Therefore, in schemes that did not have close to 50%  
581 connectivity KCs did not receive sufficiently distinct inputs. We found that while the  
582 inputs were indeed maximally separated at 50% connectivity, once the summed inputs  
583 underwent a KC threshold function all connectivity regimes were equally good at  
584 separating odors. This is in line with more recent studies that show that even a 5%  
585 connection probability generates a large representation space such that even highly  
586 similar odors are mapped to distant locations (Litwin-Kumar et al. 2017). However, these  
587 observations are confined to odor representations that are static. When the temporal  
588 patterning of inputs was included, denser connectivities appeared to be significantly  
589 better at separating odor representations.

590

591 ***Odor representations are variable in networks with dense connectivity***

592 Increasing connection density comes at a price. Odorants are embedded in a noisy and  
593 changing milieu. Recognition of appetitive and aversive odorants must play out against a  
594 background of irrelevant olfactory information. Thus, the network must be tolerant to  
595 perturbations in the odor representation. This constraint introduces an upper bound on  
596 the density of connections between PNs and KCs. Our simulations demonstrated that  
597 high connectivity values led to highly variable representations of the odor by KCs as was

598 seen from the standard deviation of the Hamming distance. Dense (80–95%)  
600 connectivity regimes generated representations that were 4–5 times more variable  
601 than representations generated by sparse connectivity schemes. The reason for this  
602 increased variability is that for dense connectivity schemes, KCs see nearly identical  
603 input from PNs. For connectivity regimes > 50%, with temporally varying PN inputs, the  
604 discriminability between KC inputs decreases with increasing connection density. The  
605 response of KCs is modulated by inhibitory feedback from the GGN. The GGN inhibits all  
606 the KCs and maintains sparseness across large variations in odor attributes by controlling  
607 the propensity of KCs to respond. In high connectivity regimes, a threshold that causes  
608 one of the KCs to fire invariably allows most KCs to fire. A small increase in threshold can  
609 lead to a condition where none of the KCs fire. Noisy changes in input statistics can thus  
610 drive the KC responses leading to large trial-trial variability. While the variability of the  
611 odor representation is maximal for connection densities in the 80-95% range, as  
612 mentioned previously even networks with connection densities in the range of 45-60%  
613 show poor classification ability when exposed to multiple trials of the same odor. This is  
614 clearly not ideal for a system attempting to represent sensory information in a  
615 stereotyped way over different trials and learn from experience.

615 ***Temporal patterning of PN activity reveals functional differences amongst PN-KC***  
616 ***connectivity regimes***

617 A key insight from the simulations performed in this paper is the observation that the  
618 categorization of odors in the insect MB is dependent on an interaction between PN-KC  
619 connectivity and temporal patterning of PN input. The reason for these differences as  
620 shown earlier is due to the differing demands of connectivity regimes on the temporal  
621 coincidence of spiking and spike thresholds. Taken together, our results reiterate that

622 temporal patterning of PN input carries information about the identity of odors (Stopfer,  
623 Jayaraman and Laurent, 2003). But more importantly, we show that this information can  
624 be utilized differently by systems with different PN-KC connectivity values. Sparse  
625 connectivity regimes utilize this in a way that allows for reduction in noise sensitivity and  
626 dense connectivity regimes use it to maximally separate between odors. Given the  
627 complexity of our sensory world, the olfactory system must balance two seemingly  
628 conflicting goals. Resolve highly similar sensory inputs and do so with considerable  
629 reliability in spite of noisy variations in the input. Our model suggests that the locust and  
630 drosophila live in different regimes of a continuum of possibilities, arriving at different  
631 solutions, perhaps driven by their own evolutionary histories. Importantly, the  
632 differences in the functions of these two circuits is only revealed when the temporal  
633 structure of the odor representation is taken into account.

634

635

**636 References :**

637 Albus, James S. 1971. A Theory of Cerebellar Function. *Mathematical Biosciences* 10  
638 (1): 25–61.

639 Aso, Yoshinori, Divya Sitaraman, Toshiharu Ichinose, Karla R. Kaun, Katrin Vogt,  
640 Ghislain Belliard-guérin, Pierre-Yves Plaçais, et al. 2014. Mushroom Body Output  
641 Neurons Encode Valence and Guide Memory-Based Action Selection in *Drosophila*.  
642 *eLife*, no. 3: 1–42.

643 Bazhenov, Maxim, Mark Stopfer, Mikhail Rabinovich, Henry D. I. Abarbanel, Terrence J.  
644 Sejnowski, and Gilles Laurent. 2001. Model of Cellular and Network Mechanisms for  
645 Odor-Evoked Temporal Patterning in the Locust Antennal Lobe. *Neuron* 30 (2): 569–  
646 81.

- 647 Caron, Sophie J. C., Vanessa Ruta, L. F. Abbott, and Richard Axel. 2013. Random  
648 Convergence of Olfactory Inputs in the *Drosophila* Mushroom Body. *Nature* 497  
649 (7447): 113–17.
- 650 Cassenaer, Stijn, and Gilles Laurent. 2012. Conditional Modulation of Spike-  
651 TimingDependent Plasticity for Olfactory Learning. *Nature* 487 (7405): 128–128.
- 652 Destexhe, A., Z. F. Mainen, and T. J. Sejnowski. 1994. An Efficient Method for Computing  
653 Synaptic Conductances Based on a Kinetic Model of Receptor Binding. *Neural*  
654 *Computation* 6 (1): 14–18.
- 655 Dhawale, Ashesh K., Akari Hagiwara, Upinder S. Bhalla, Venkatesh N. Murthy, and Dinu  
656 F. Albeanu. 2010. Non-Redundant Odor Coding by Sister Mitral Cells Revealed by  
657 Light Addressable Glomeruli in the Mouse. *Nature Neuroscience* 13 (11): 1404–12.
- 658 Fisek, Mehmet. 2014. Connectivity and Computations in Higher-Order Olfactory Neurons  
659 in *Drosophila*. <https://dash.harvard.edu/handle/1/12274607>.
- 660 Gruntman, Eyal, and Glenn C. Turner. 2013. Integration of the Olfactory Code across  
661 Dendritic Claws of Single Mushroom Body Neurons. *Nature Neuroscience* 16 (12):  
662 1821–29.
- 663 Hallem, Elissa A., and John R. Carlson. 2004. The Odor Coding System of *Drosophila*.  
664 *Trends in Genetics: TIG* 20 (9): 453–59.
- 665 Hallem, Elissa A., and John R. Carlson.. 2006. Coding of Odors by a Receptor Repertoire.  
666 *Cell* 125 (1): 143–60.
- 667 Heisenberg, Martin. 2003. Mushroom Body Memoir: From Maps to Models. *Nature* 4  
668 (April): 266–75.
- 669 Hige, Toshihide, Yoshinori Aso, Mehrab N. Modi, Gerald M. Rubin, and Glenn C. Turner.  
670 2015. Heterosynaptic Plasticity Underlies Aversive Olfactory Learning in *Drosophila*.  
671 *Neuron* 88 (5): 985–98.
- 672 Hige, Toshihide, Yoshinori Aso, Gerald M. Rubin, and Glenn C. Turner. 2015. Plasticity-  
673 Driven Individualization of Olfactory Coding in Mushroom Body Output Neurons.  
674 *Nature* 526 (10): 258–62.
- 675 Hopfield, J. J., and D. W. Tank. 1986. Computing with Neural Circuits: A Model. *Science*  
676 233 (4764): 625–33.

- 677 Jortner, Ron A. 2013. Network Architecture Underlying Maximal Separation of Neuronal  
678 Representations. *Frontiers in Neuroengineering* 5 (January): 19.
- 679 Jortner, Ron A., S. Sarah Farivar, and Gilles Laurent. 2007. A Simple Connectivity Scheme  
680 for Sparse Coding in an Olfactory System. *Journal of Neuroscience* 27 (7):  
681 1659–69.
- 682 Kazama, Hokto, and Rachel I. Wilson. 2009. Origins of Correlated Activity in an Olfactory  
683 Circuit. *Nature Neuroscience* 12 (9): 1136–44.
- 684 Kristan, William B., and Paul Katz. 2006. Form and Function in Systems Neuroscience.  
685 *Current Biology: CB* 16 (19): R828–31.
- 686 Laurent, Gilles. 1996a. Dynamical Representation of Odors by Oscillating and Evolving  
687 Neural Assemblies. *Trends in Neurosciences* 19 (11): 489–96.
- 688 Laurent, Gilles. 1996b. Temporal Representations of Odors in an Olfactory. *The Journal*  
689 *of Neuroscience* 16 (12): 3837–47.
- 690 Lin, Andrew C., Alexei M. Bygrave, Alix de Calignon, Tzumin Lee, and Gero Miesenböck.  
691 2014. Sparse, Decorrelated Odor Coding in the Mushroom Body Enhances Learned  
692 Odor Discrimination. *Nature Neuroscience* 17 (4): 559–68.
- 693 Litwin-kumar, Ashok, Kameron D. Harris, Richard Axel, and Larry F. Abbott. 2017.  
694 Optimal Degrees of Synaptic Connectivity. *Neuron*, 93(5), 1153-1164
- 695 Marr, D. 1969. A Theory of Cerebellar Cortex. *The Journal of Physiology* 202 (2): 437–  
696 70.
- 697 Masuda-Nakagawa, Liria M., Kei Ito, Takeshi Awasaki, and Cahir J. O’Kane. 2014. A  
698 Single GABAergic Neuron Mediates Feedback of Odor-Evoked Signals in the  
699 Mushroom Body of Larval *Drosophila*. *Frontiers in Neural Circuits* 8 (April): 35.
- 700 Mazor, Ofer, and Gilles Laurent. 2005. Transient Dynamics versus Fixed Points in Odor  
701 Representations by Locust Antennal Lobe Projection Neurons. *Neuron* 48: 661–73.
- 702 Oswald, David, Johannes Felsenberg, Clifford B. Talbot, Gaurav Das, Emmanuel Perisse,  
703 Wolf Huetteroth, and Scott Waddell. 2015. Activity of Defined Mushroom Body  
704 Output Neurons Underlies Learned Olfactory Behavior in *Drosophila*. *Neuron* 86  
705 (2): 417–27.

- 706 Papadopoulou, Maria, Stijn Cassenaer, Thomas Nowotny, and Gilles Laurent. 2011.  
707 Normalization for Sparse Encoding of Odors by a Wide-Field Interneuron. *Science*  
708 721 (6030): 721–25.
- 709 Perez-Orive, Javier, Ofer Mazor, Glenn C. Turner, Stijn Cassenaer, Rachel I. Wilson, and  
710 Gilles Laurent. 2002. Oscillations and Sparsening of Odor Representations in the  
711 Mushroom Body. *Science* 297 (July): 359–66.
- 712 Perez-Orive, J., Maxim Bazhenov, and Gilles Laurent. 2004. Intrinsic and Circuit  
713 Properties Favor Coincidence Detection for Decoding Oscillatory Input. *Journal of*  
714 *Neuroscience* 24 (26): 6037–47.
- 715 Saha, Debajit, Wensheng Sun, Chao Li, Srinath Nizampatnam, William Padovano,  
716 Zhengdao Chen, Alex Chen, et al. 2017. Engaging and Disengaging Recurrent  
717 Inhibition Coincides with Sensing and Unsensing of a Sensory Stimulus. *Nature*  
718 *Communications* 8 (May): 15413.
- 719 Stopfer, Mark, Vivek Jayaraman, and Gilles Laurent. 2003. Intensity versus Identity  
720 Coding in an Olfactory System. *Neuron* 39 (6): 991–1004.
- 721 Tanaka, Nobuaki K., Kei Ito, and Mark Stopfer. 2009. Odor-Evoked Neural Oscillations in  
722 *Drosophila* Are Mediated by Widely Branching Interneurons. *The Journal of*  
723 *Neuroscience* 29 (26): 8595– 8603.
- 724 Turner, Glenn C., Maxim Bazhenov, and Gilles Laurent. 2008. Olfactory Representations  
725 by *Drosophila* Mushroom Body Neurons. *Journal of Neurophysiology* 99: 734–46.
- 726 Wehr, M., and G. Laurent. 1996. Odour Encoding by Temporal Sequences of Firing in  
727 Oscillating Neural Assemblies. *Nature* 384 (6605): 162–66.
- 728 Wiechert, Martin T., Benjamin Judkewitz, Hermann Riecke, and Rainer W. Friedrich.  
729 2010. Mechanisms of Pattern Decorrelation by Recurrent Neuronal Circuits. *Nature*  
730 *Neuroscience* 13 (8): 1003–10.
- 731 Wilson, Rachel I., and Gilles Laurent. 2005. Role of GABAergic Inhibition in Shaping  
732 Odor-Evoked Spatiotemporal Patterns in the *Drosophila* Antennal Lobe. *The Journal*  
733 *of Neuroscience* 25 (40): 9069–79.
- 734 Yasuyama, Kouji, and Paul M. Salvaterra. 1999. Localization of Choline  
735 Acetyltransferase-Expressing Neurons in *Drosophila* Nervous System. *Microscopy*  
736 *Research and Technique* 45 (2): 65–79.

## Figure Captions

737

738

739

Figure 1: A schematic of the insect olfactory system

740

A schematic of the olfactory system contrasting the structural parameters of the circuit in a) *Drosophila melanogaster* and b) *Schistocerca americana*.

741

742

743

Figure 2: 50% connectivity does not maximally separate KC representations when PN inputs are static

744

745

a) The threshold model of KCs. The left-most vector represents the PN activity. This is combined through a connectivity matrix to give the input seen by each KC (a 50000-element long vector). Thresholding is then applied to define spiking KCs. b) The Hamming distance between inputs seen by two KCs is calculated for all possible pairs and averaged and plotted as a function of the PN-KC connectivity. c) The mean ( $\pm$  standard deviation) normalized Hamming distance between the activity of KC networks driven by two different inputs is plotted on the y-axis as a function of the PN-KC connectivity. Different shades plot the distance between odor representations that differed in 5-80% of the active PNs.

746

747

748

749

750

751

752

753

754

755

Figure 3: Simulation of temporally patterned PN inputs to a KC network.

756

757

a) The matrix on the left represents the activity of a set of 900 PNs. Each row shows the activity of a single PN during a 3000ms time period. Blue dots show the time of a spike. The red region represents the time during which the odor was presented. On top, a summation of the activity of the entire PN network is shown clearly indicating

758

759

760

the oscillations in the net PN activity. This input was used to calculate  $T$  and  $I_{syn}$  (the synaptic input to KCs). The differences between the population representation of two inputs were calculated using the Hamming distance. b) Mean population response of 900 PNs projected onto the first three principal components for three odors is shown by the black traces. Individual trials are shown by the colored traces c) The mean membrane potential of all KCs shows a 20Hz oscillation. Bottom panels show the response of two KCs (in red and black traces) to two different odors. Only the first odor evokes a consistent response from this particular KC across 5 odor trials (middle panel). The second odor does not lead to reliable spiking in this example KC.

761

762

763

764

765

766

767

768

769

770

Figure 4: PN temporal patterning reveals the functional differences between connectivities

771

772

a) Distance between odor representations. The mean ( $\pm$  standard deviation) normalized Hamming distance between the KC representations of odor pairs is shown as a function of the PN-KC connectivity value. Here KCs are modeled as described in Figure 3. b) Classification accuracy decreases with increasing PN-KC connectivity. A  $k$ -medoids clustering algorithm that used the distance between 25 KC activity vectors (5 trials  $\times$  5 odors) was used to categorize each vector as one of 5 odors. The percentage of correctly classified odor representations is plotted on the y-axis as a function of the connectivity of the PN-KC network. c) Odor representations become indistinguishable with increasing PN-KC connectivity. Five odors that differed from each other by 5% PN

773

774

775

776

777

778

779

780

30



781 *input, mapped to a plane using multidimensional scaling. Different trials of a given odor*  
782 *are plotted using a single color. Different odors are plotted using different colors. The*  
783 *PN-KC connectivity is shown in the title of each sub-plot d) Hamming distance between*  
784 *static odor representations. The mean ( $\pm$  standard deviation) normalized Hamming*  
785 *distance between the KC representations of odor pairs is plotted as a function of PN-KC*  
786 *connectivity. Here, the PN odor representation did not change in time.*

787

788 *Figure 5: Glomerular organization of the fly aids odor discrimination*

789 *(a) The mean ( $\pm$  standard deviation) normalized Hamming distance as a function of PN-*  
790 *KC connectivity in a network with glomerular structure. (b) The normalized HD of odors*  
791 *with a 1-glomerulus difference in a fly-like glomerular system is compared to the HD*  
792 *between odor representations of a system with locust-like glomerular structure. (c)*  
793 *Classification accuracy of odors that are different by 2 glomeruli (2% or 12 neurons in the*  
794 *fly-architecture) (blue trace) compared to the classification accuracy of odors that*  
795 *differed by 5% (45 neurons) of stimulated odors in locust. Classification accuracy is higher*  
796 *for the fly-like organization for low PN-KC connectivities.*

797

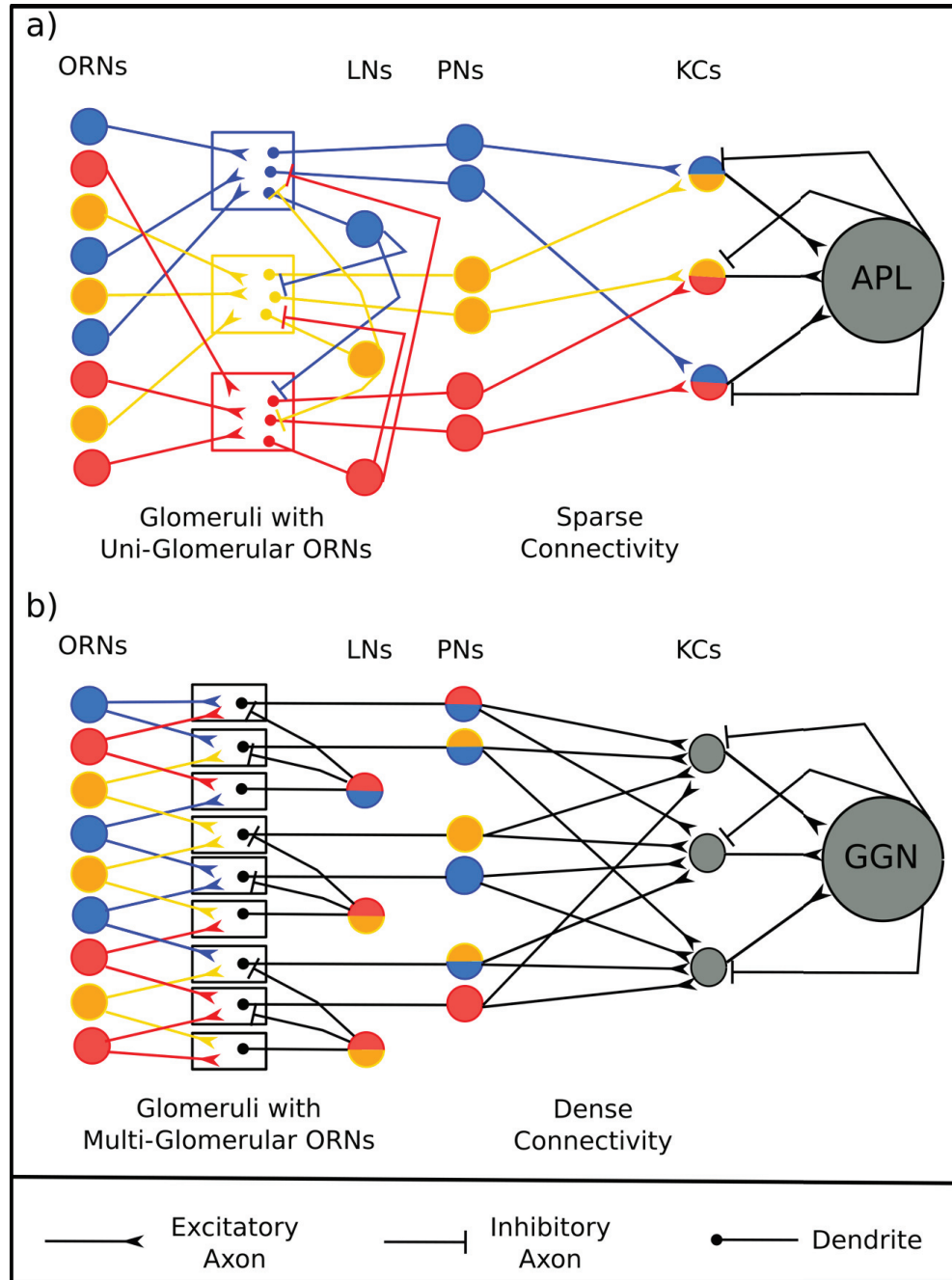
798 *Extended Data 1 : Code to simulate PN and KC networks.*

799 *The included .zip file contains MATLAB code used in the paper to produce PN network*  
800 *responses and simulated the KC network.*



801 754 **Figure 1**

802 755



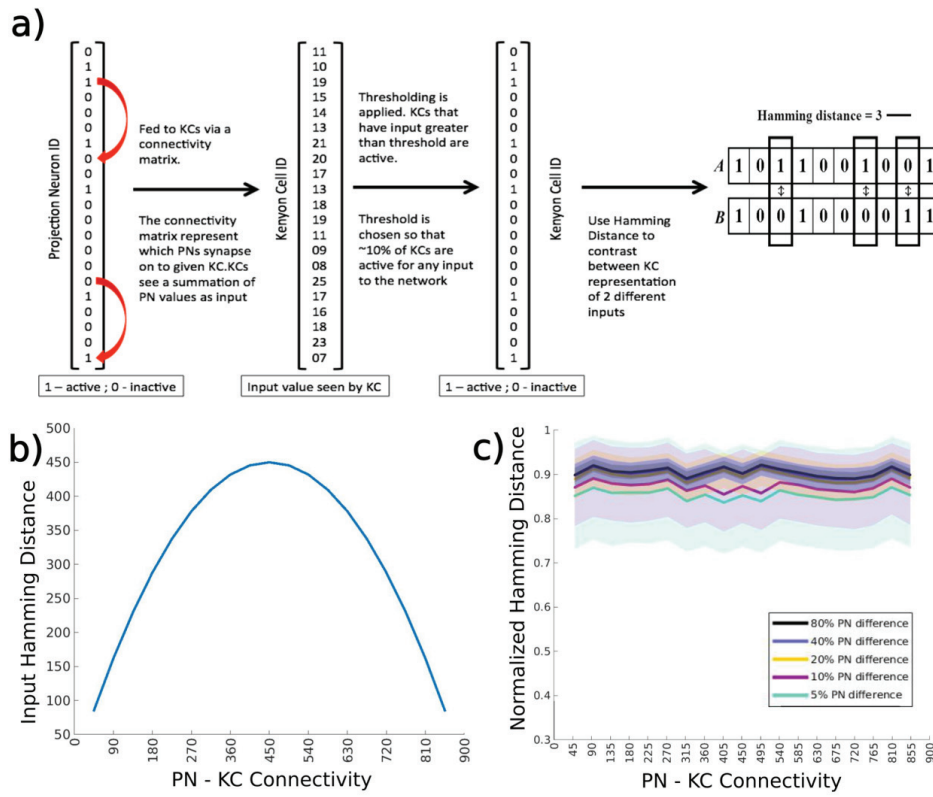
803

804

806

806 757 **Figure 2**

809



808

809

810

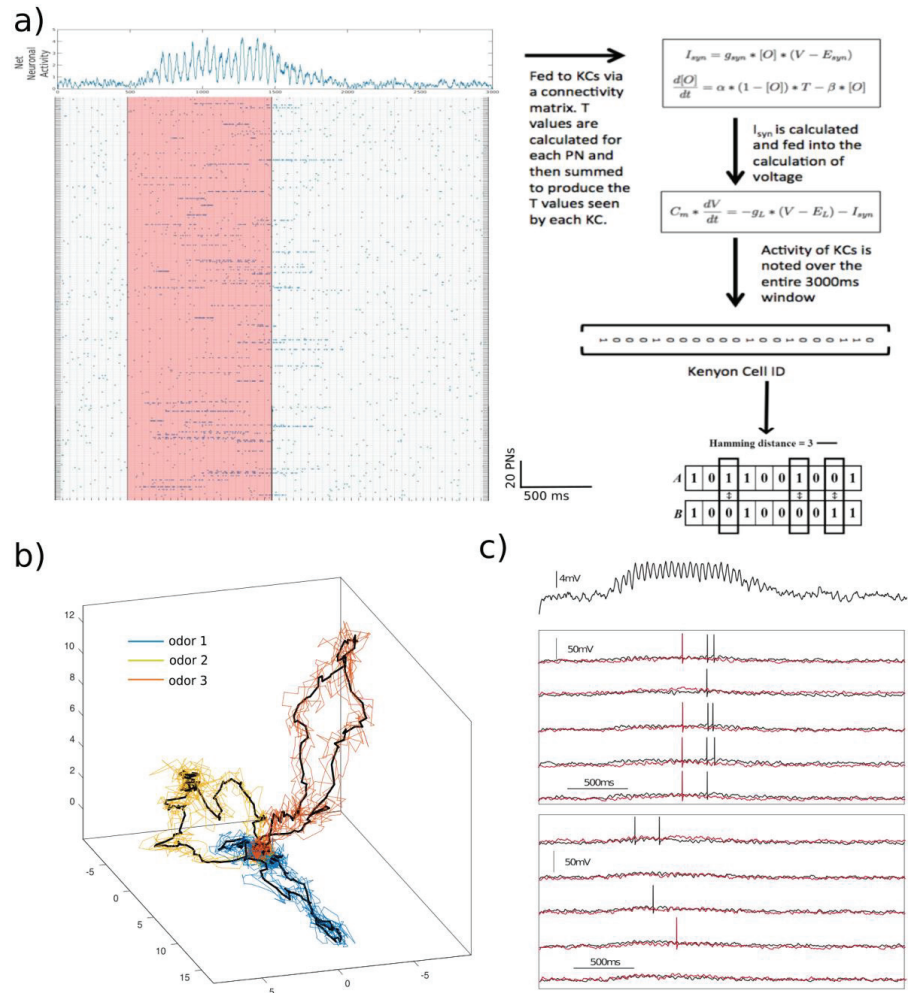
811

812

813

814

815 760 **Figure 3**



816 761

817

818

819

820

821

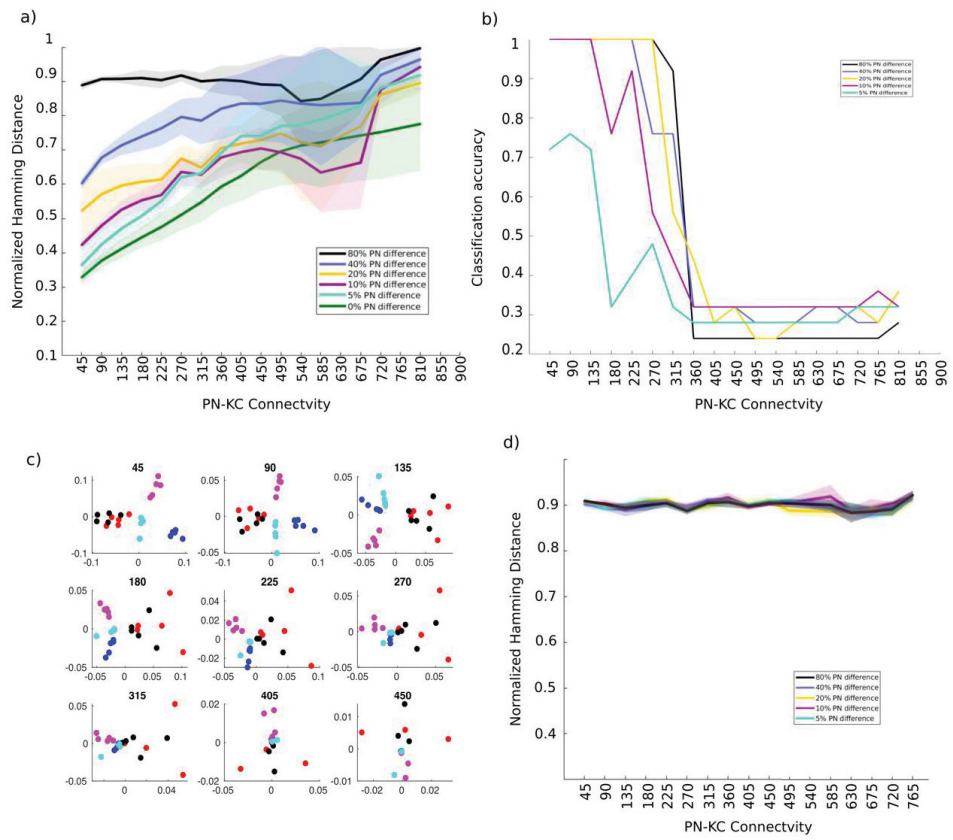
34

822

823

824 763 **Figure 4**

825 764



826

827

828

829 766 **Figure 5**

830 767

